



Interpretation Target Pattern of a Buried Basic Object on Surface Ground Penetrating Radar System

Nana Rachmana, Hendrawan, Sugihartono, Andriyan B Suksmono.

School of Electrical Engineering and Informatics, Institut Teknologi Bandung, Indonesia

e-mail: nana@telecom.ee.itb.ac.id

Abstract: Surface Ground Penetrating Radar (GPR) is the one of Radar technology that is widely used on many applications. It is non-destructive remote sensing method to detect underground buried objects. However, the output target is only hyperbolic representation. This research tries to enhance GPR capability by representing the visual/pattern of the detected target. GPR data of many basic objects (with circular, triangular and rectangular cross-section) are classified and extracted to generate data training model as a unique template for each type basic object. The pattern of object under test will be known by comparing its data with the training data using a decision tree method. A simple powerful algorithm to extract feature parameters of object which based on linier extrapolation is proposed. The result shown that tested buried basic objects can be correctly interpreted.

Keywords: GPR, object interpretation, extract feature.

1. Introduction

Surface Ground Penetrating Radar (GPR) which has evolved as popular technology for non destructive testing method has been widely used for the detection of underground buried objects since 1980s. GPR transmits short pulses of high frequency electromagnetic into the ground. These waves propagate with a velocity that depends on the dielectric property of medium. If the waves encounter a buried object with different reactive indices, some of the waves are reflected back and the receiver processes them to create a hyperbolic image as the object representation. In order to create an image, the GPR transmits electromagnetic pulses at a certain frequency for a certain time slot and samples the responses as an A-scan corresponding to a single position of the GPR. By moving the GPR in x direction, a collection of these A-scans called a B-scan which representing different GPR positions are constructed. Then it is processed become a hyperbolic image. Ideally, the imaging process of GPR data is described in Figure 1.

Figure 2 shows the B-scan of GPR data for basic circular and rectangular objects. From the image, it is hard to recognize the shape of the object. Image of an object generated by GPR is not corresponding to its geometrical representation. Regeneration of a geometric model is a much more complex procedure and is not usually attempted [1]. However, due to output target is only a hyperbolic representation, interpretation of a geometric buried object is depends on operator's expertise and experience.

Recent developments have shown that significant efforts have been focused towards the extraction of meaningful physical interpretation from GPR data. Researches on generating geometrical representation have been reported by Devaney [2], Johansson and Mast [3]; Laksameethansan [4]. Unfortunately, these reports based on diffraction tomography or cross-hole GPR method, which not practical to drill holes and time consumed.

For interpreting buried object like pipes, tunnels and Anti-personnel landmines in subsurface images, a variety of techniques applying the Hough transform method is widely used [5]. The latest and newest technique using compressive sensing for GPR imaging has been reported [6]. Those techniques are still high computational cost and hard to be implemented in on-line or riel time processing.

This research tries to interpret geometrical representation from B-scan of GPR data based on template matching. The pattern of object under test will be interpreted by comparing its data with the training data using a simple decision tree method. The objective of the research in the medium term is enhancement of GPR capability by representing the visual/pattern of the detected target. The idea is illustrated in figure 3.

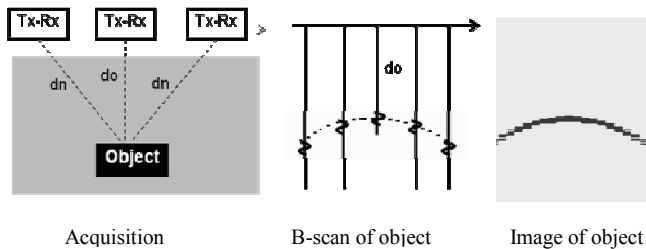


Fig.1 Imaging Process of GPR data

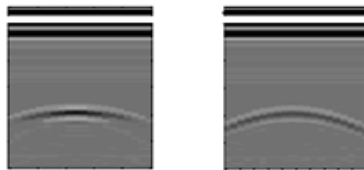


Fig.2 B-scan of GPR data for basic circular and rectangular

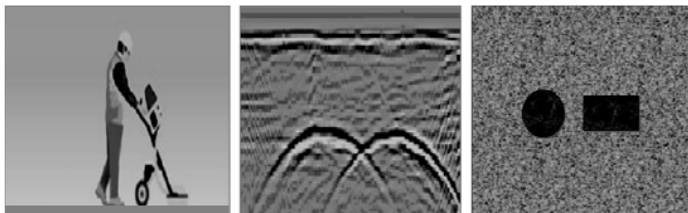


Fig.3 Enhancement of GPR output from hyperbolic to visual representation

2. The GPR test range model

The model GPR test range is a box with 3 meter length, 3 meter wide and 2 meter high (3x3x2 meter), contains a half full of sand. A 1GHz transmitter and receiver of GPR, which has 10 centimetre fix-distance and located 20 centimetre above the sand, moves to X direction in 5 centimetre intervals until 1meter length (20 scan positions). In each interval, pulse signal which 12 ns duration transmitted. The sand has parameter relative permittivity is 3.0, conductivity is 10^{-2} Siemens/meter, and relative permeability is 1. A simple buried object (with three type patterns: circular, triangular or rectangular cross-section) is made from perfect conductor material is lied in the sand at 50 cm depth. Figure 4 shows the model of simulation.

For training purpose, 30 samples of three types (circular, triangular and rectangular) object data are generated. For each type object data has 10 different size samples. Test data consist of 12 samples of the three type object which each type has 4 different sample sizes.

In the GPR modelling, a mathematical modelling has become a rapidly popular interpretation tool and is widely used in conjunction with many image processing techniques.

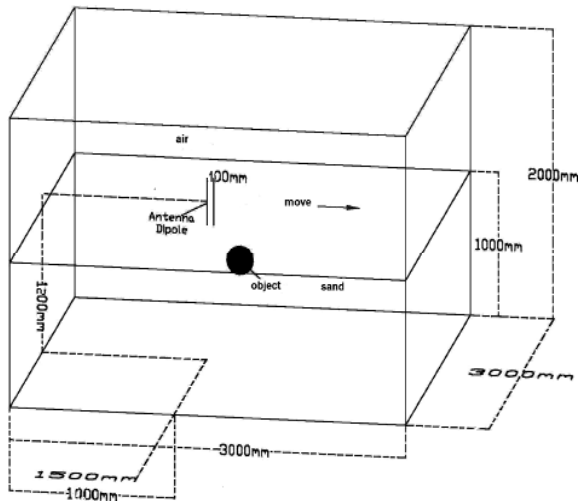


Fig.4 GPR test range model

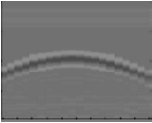
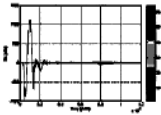
Input : a circular object	Output: a file *a.out	a file*b.out. E _z scans and plots using MATLAB
<pre> #medium: 3.0 0.0 0.0 0.01 1.0 0.0 sand ----- #domain: 3.0 2.0 #dx_dy: 0.01 0.01 #time_window: 12e-9 ----- #box: 0.0 0.0 3.0 1.0 sand #cylinder: 1.5 0.4 0.1 pec ----- #scan: 20 1.0 1.2 0.05 0.0 1.1 1.2 0.05 0.0 1.0 1.0e9 sine CIR#0_10b.out b ----- #geometry_file: CIR#0_10b.geo #title: circular object model #messages: y </pre>	<pre> #GprMax2D, Ver 1.5 Rev.2 #title: circular object model in sand #iterations: 509 #DX: 0.01 metre #DY: 0.01 metre #DT: 2.358e-09 #Number of antennas: 1 #scan: 20 1.0 1.2 0.05 0.0 1.1 1.2 0.05 sine </pre> <div style="border: 1px solid black; padding: 5px; width: fit-content; margin: 10px auto;"> <p>Each file has 10180 rows data</p> </div> <pre> TX at : 0015 00120, RX at : 00115 00120 TIME (NS) EX (V/m) EX (A/m) HY (A/m) +0.00000e+00 +0.00000e+00 +0.00000e+00 +0.00000e+00 +2.35865e-02 +0.00000e+00 +0.00000e+00 +0.00000e+00 +4.71731e-02 +0.00000e+00 +0.00000e+00 +0.00000e+00 +7.07596e-02 +0.00000e+00 +0.00000e+00 +0.00000e+00 +9.43462e-02 +0.00000e+00 +0.00000e+00 +0.00000e+00 +1.17933e-01 +0.00000e+00 +0.00000e+00 +0.00000e+00 +1.41519e-01 +0.00000e+00 +0.00000e+00 +0.00000e+00 +1.65106e-01 +0.00000e+00 +0.00000e+00 +0.00000e+00 +1.88692e-01 +0.00000e+00 +0.00000e+00 +0.00000e+00 +2.12279e-01 +0.00000e+00 +0.00000e+00 +0.00000e+00 +2.35865e-01 +0.00000e+00 +0.00000e+00 +0.00000e+00 +2.59452e-01 +0.00000e+00 +0.00000e+00 +0.00000e+00 +2.83038e-01 -1.92590e+00 +3.61483e+03 +1.79156e-02 +3.06625e-01 -3.80957e+00 -9.11636e-03 +1.70995e-01 +3.30212e-01 -5.18314e+01 +4.88417e-02 +3.76354e-01 +3.53798e-01 -9.87165e+01 -2.35021e-02 +1.00544e+00 +3.77385e-01 -3.17852e+02 +1.02810e-01 +1.71708e+00 +4.00971e-01 -5.30018e+02 +1.11528e-01 +2.34036e+00 +4.24558e-01 -7.51751e+02 +4.22328e-02 +2.82184e+00 +4.48144e-01 -9.57002e+02 +2.01777e-01 +2.78803e+00 +4.71731e-01 -9.07277e+02 +1.47463e-01 +2.67887e+00 +4.95317e-01 -8.37664e+02 +6.72124e-02 +2.78650e+00 +5.18904e-01 -8.55610e+02 +1.61598e-01 +2.90974e+00 +5.42490e-01 -8.54798e+02 +1.91622e-01 +2.79286e+00 +5.66077e-01 -7.92935e+02 +7.72128e-02 +2.51783e+00 +5.89664e-01 -7.13688e+02 +9.24497e-02 +2.21036e+00 +6.13250e-01 -5.77958e+02 +1.60353e-01 +1.95383e+00 +6.36837e-01 -4.29555e+02 +9.53088e-02 +1.68660e+00 +6.60423e-01 -3.33900e+02 +1.54310e-01 +1.29783e+00 +6.84010e-01 -2.30923e+02 +6.67077e-02 +7.83453e-01 +7.07596e-01 -3.31163e+01 +7.95314e-02 +3.23215e-01 +7.31183e-01 +1.65418e+02 -1.44620e-02 -3.61834e-02 +7.54770e-01 +2.75217e+02 -5.34592e-02 -4.46616e-01 +7.78356e-01 +3.78985e+02 +4.43086e-04 -9.77479e-01 +8.01943e-01 +5.64460e+02 -2.34835e-02 -1.44818e+00 +8.25529e-01 +7.37562e+02 -1.12051e-01 -1.76413e+00 +8.49116e-01 +8.16947e+02 -1.17961e-01 -2.06395e+00 </pre>	 <p>Scanned file *b.out</p>  <p>plotted file *b.out</p>

Fig.5 An input and an output GPR data simulator

In general, the mathematical modelling methods can be classified into two approaches there are methods of moment and discrete element methods. However, the last method which is known as the finite-difference time-domain (FDTD) has become one of the most popular used in the past few years, especially with the rapid increase in accessible and inexpensive computational resources. There are a lot of different electromagnetic FDTD formulas, each with individual strength and weaknesses.

Successful GPR modelling based on the finite-difference time-domain has been reported by many authors such as developed by Antonis Giannopoulos of the University of Edinburgh [7] and James Irving of the Stanford University [8]. Giannopoulos has developed GPR modelling facilities called GprMax2D/3D ver. 2.0 which is used to generate the GPR data. The output simulator can be a file*b.out and file*a.out to represent hyperbolic image in binary file and ASCII file respectively. Sampling experiment by using riel GPR tool will be done in GPR test range ICTR-ITB laboratory to validate and verify the GPR data simulator. An example of input and output GPR data simulator is shown in figure 5. The research takes files*a.out as input of the proposed system to generate training data and test data files.

3. Proposed system

The proposed system for object classification and interpretation describes as in figure 6. Firstly an output GPR (a file*a.out) is extracted to generate reflected signal $E_{(z)}$ (V/m) as function of time (ns). Based on observations, others reflected signal such as $H_{(x)}$ and $H_{(y)}$ are neglected because of no significant difference between these three types object.

The difference of the output GPR format and the input of C.45 software tool [9] need to generate a program to convert those formats. The program is based on Java called *DataCreator*, *NamesCreator*, *TstCreator*, and *AhCreator* generates a file*.data, a file*.names, a file*.tst and file*.ah respectively. The first two files are needed to generate the training data and the last two file to generate and to test the test data.

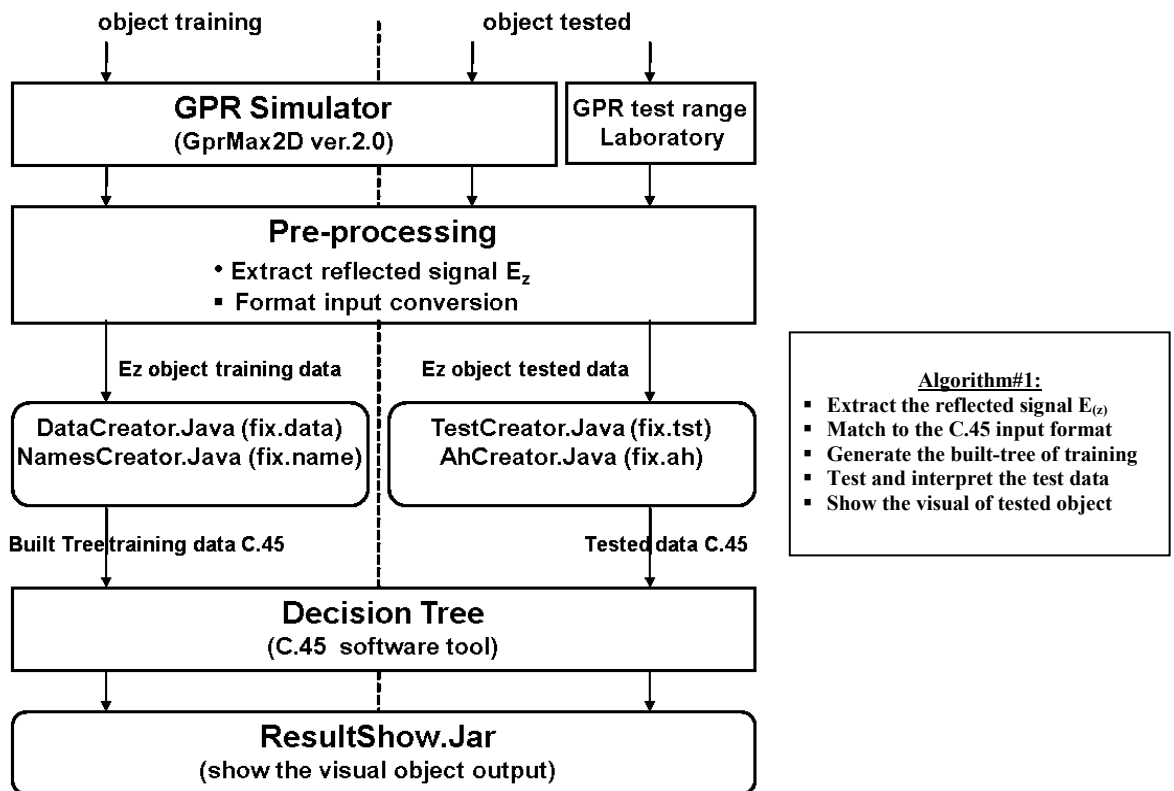


Fig. 6 The proposed system and the algorithm#1

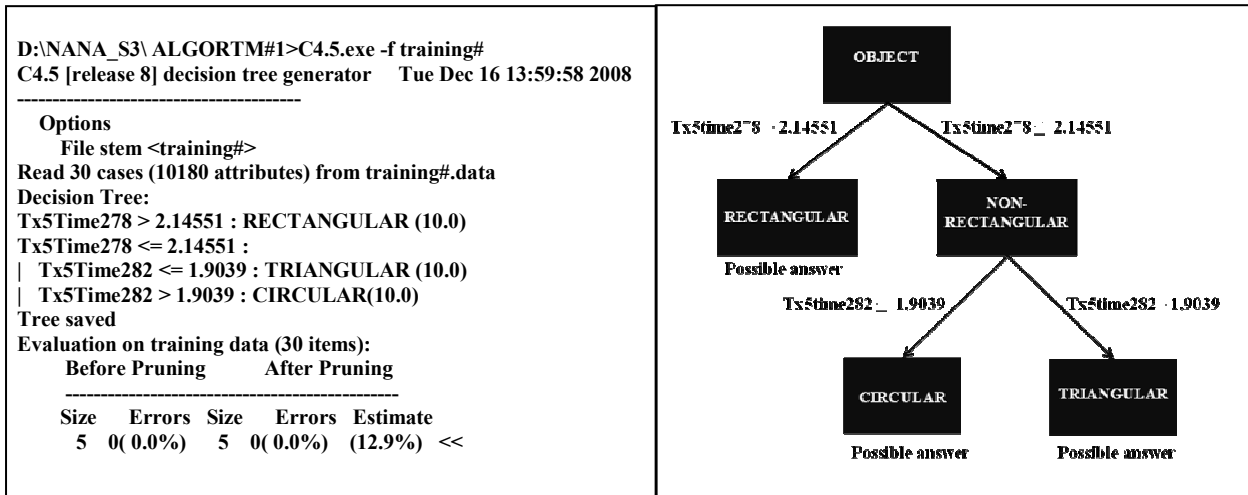


Fig.7 The Built-tree of the training data

The C.45 software tool needs built-tree of training data to predict a decision. Generation of built-tree can be done after file*.data and file*.names have been generated. Values of training data are calculated to determine entropy and gain ratio for each attribute. Entropy is used to measure how informative is a node in a tree and gain ranks attributes and to build a decision tree of the training data.

Interpretation of a test data (an unknown object) can be done after the file*.tst is generated. By the decision tree records that have unknown attribute values can be classified by estimating the probability of the various possible results.

Finally the ResultShower.jar program converts the output decision of C.45 in text form to visual pattern form to show the visual of the tested unknown object. These Steps of the process is summarized in algorithm #1.

An example in this experiment, training data consist of 30 samples of three type (circular, triangular and rectangular) object data. For each type object data has 10 different size samples (r:7,10,12,13,15,17,18,19,20 and 23). Each sample has 10180 attributes of the file*.data, so, the training data totally has 305400 attributes. Figure 7 shows the built-tree of the training data.

A. Testing Scenarios

There are scenarios cover both for same environment test condition and different environment test condition. The test data for each scenario consist of 12 samples of the three type object which each type has 4 different sample sizes (r: 8,9,21 and 22). The total sample test data for all scenarios are 96 samples. These scenarios are:

1). Tested and training objects are in the same depth condition (50 centimetre):

Scenario #0: the sand and the tested object have same parameters as in the training data (the sand: $\epsilon_r=3$, $\mu_r=1$, and the object: perfect conductor). Tested and training objects have same environmental condition.

Scenario #1: the sand has same parameter as in training data and the tested object has different material (the sand: $\epsilon_r=3$, $\mu_r=1$, and the object: fresh water, $\rho_r=81$).

Scenario #2: the tested object has same parameter as training data and the sand has different permittivity (sand: $\epsilon_r=4$, $\mu_r=1$, and the object: perfect conductor).

Scenario #3: the sand medium and the tested object have different parameters compare to training data (sand: $\epsilon_r=4$, $\mu_r=1$, and the object: fresh water, $\rho_r=81$).

2). *Tested and training objects are in the different depth condition:*

Scenario #4: the sand and the tested object have same parameters as in the training data (the sand: $\epsilon_r=3$, $\mu_r=1$, and the object: perfect conductor), and depth of the tested object is 40 cm.

Scenario #5: the sand and the tested object have same parameters as in the training data (the sand: $\epsilon_r=3$, $\mu_r=1$, and the object: perfect conductor), and depth of the tested object is 55 cm.

Scenario #6: the sand has same parameter as in training data and the object to be tested has different material (the sand: $\epsilon_r =3$, $\mu_r =1$, and the object: fresh water, $\rho_r =81$), and the depth of the tested object is 40 cm.

Scenario #7: the sand has same parameter as in training data and the tested object has different material (the sand: $\epsilon_r =3$, $\mu_r =1$, and the object: fresh water, $\rho_r =8$), and depth of the tested object is 55 cm.

B. The test result based on the algorithm #1

An example, the system interpretation using decision tree based on the algorithm #1 of the partial test result for scenario #6 is shown on figure 8 and all the test result is summarized in table 1. The result shown that from 96 tested data samples, the system can truly well interpret only for 50 samples (52%). The algorithm#1 has inaccurate interpretation for condition where the trained and the training object have different environmental condition.

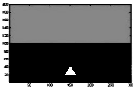
Device Under Test	Results of the interpretation
	<pre>D:\ALGORTM#1>T.exe -f training# training#.ah TRI#1_21_40.tst C4.5 [release 8] decision tree interpreter Tue Dec 16 16:20:14 2008 ----- Tx5Time278: inserting 1.151200 Tx5Time282: inserting 5.543930 Decision: CIRCULAR CF = 1.00 [0.87 - 1.00]</pre>
	<pre>D:\ALGORTM#1>T.exe -f training# training#.ah CIR#1_8_40.tst C4.5 [release 8] decision tree interpreter Tue Dec 16 16:24:10 2008 ----- Tx5Time278: inserting 2.353900 Decision: RECTANGULAR CF = 1.00 [0.87 - 1.00]</pre>
	<pre>D:\ALGORTM#1>T.exe -f training# training#.ah REC#1_9_40.tst C4.5 [release 8] decision tree interpreter Tue Dec 16 16:35:47 2008 ----- Tx5Time278: inserting 1.680600 Tx5Time282: inserting 1.186690 Decision: TRIANGULAR CF = 1.00 [0.87- 1.00]</pre>

Fig.8 An example of the partial test result for scenario #6

4. The Feature extraction

An effort to enhance the performance of the system is done by adding a feature extraction of the object to the algorithm#1. This improved algorithm called as algorithm#2. Investigation of reflected signal $E_{(z)}$ received by receiver for 30 samples of three types (circular, triangular and rectangular) object of training data carries out an important information that is for each type object has a unique pattern signal. This phenomenon can be shown in figure 9.

TABLE 1
THE TEST RESULT BASED ON THE ALGORITHM #1

DUT \ Sc#n	Sc#0	Sc#1	Sc#2	Sc#3	Sc #4	Sc#5	Sc#6	Sc#7
TRI_8	true	True	true	true	true	true	False	true
TRI_9	true	True	true	true	true	true	False	true
TRI_21	true	True	true	true	true	true	False	true
TRI_22	true	True	true	true	true	true	False	true
CIR_8	true	True	False	False	False	False	False	False
CIR_9	true	True	False	False	False	False	False	False
CIR_21	true	True	False	False	False	False	False	False
CIR_22	true	True	False	False	False	False	False	False
REC_8	true	True	False	False	true	False	False	False
REC_9	true	True	False	False	true	False	False	False
REC_21	true	True	False	False	true	False	true	False
REC_22	true	True	False	False	true	False	true	False

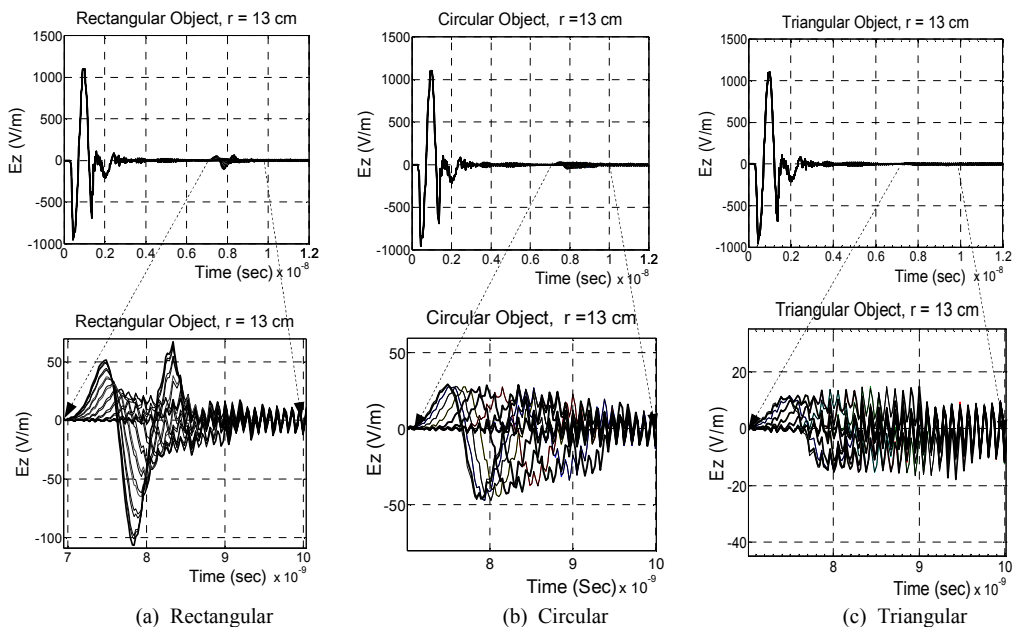


Fig.9 Received signal pattern for three type of the basic object

The unique pattern signal is extracted as the object feature. To simplify the feature and to reduce the number attribute of complex extracted signal pattern, the time variable is excluded by sorting values of the $E_{(z)}$ from the smallest to the largest, and then a linear extrapolation is applied. Changing the testing condition (ϵ_r , μ_r , ρ_r , depth) will shift the position in time and change the amplitude without change the pattern. By this process, each reflected signal pattern of an object which in algorithm#1 has 10180 attributes will be transformed to a straight line which has only 3 attributes, these are slope of the line (a), intersection point of the line with the $E_{(z)}$ axis (b) and standard deviation (s). Furthermore, these attributes are used as the object representation. Figure 10 shows the algorithm#2 and its illustration.

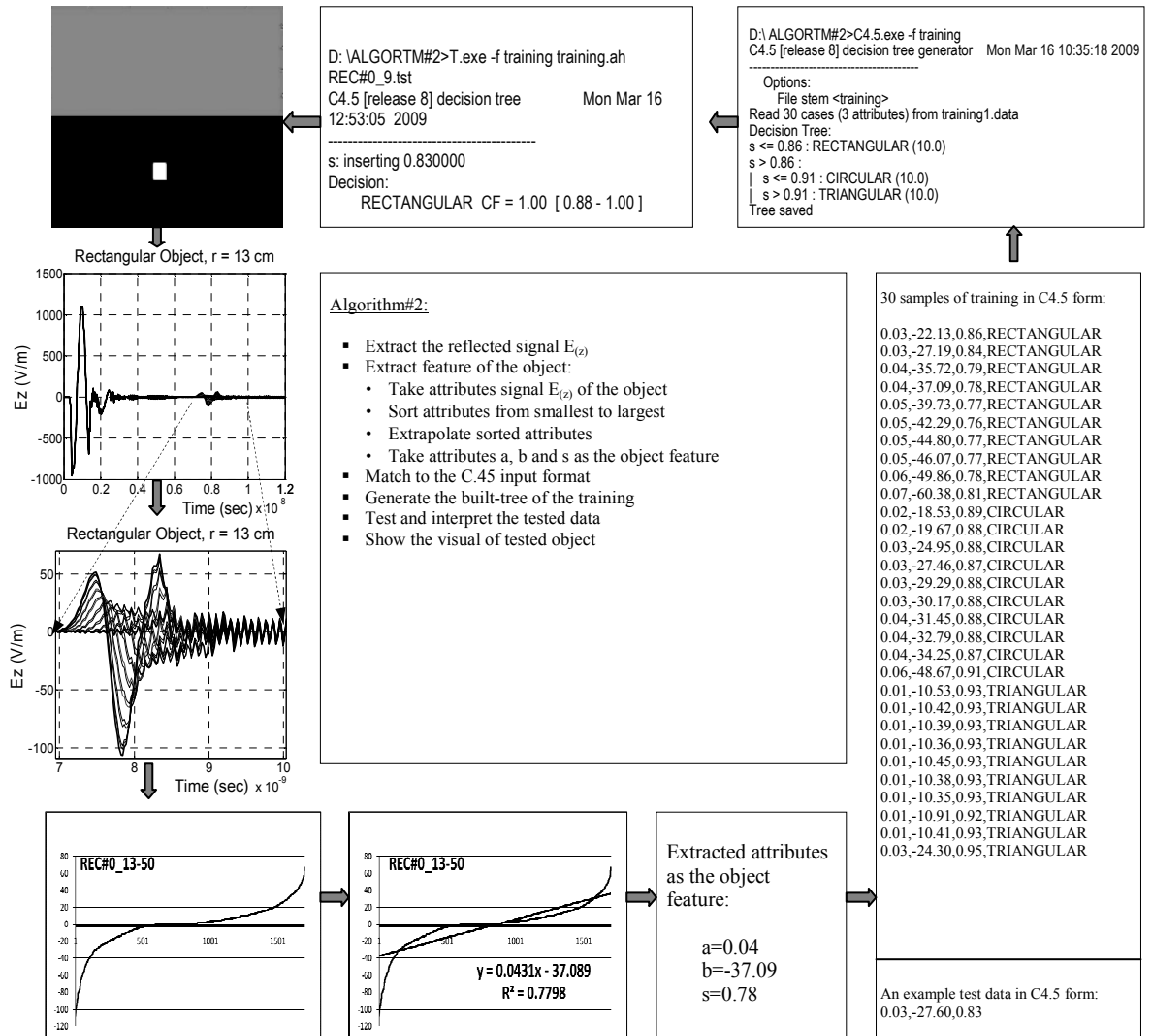


Fig.10 The proposed algorithm#2 and its illustration

A. The test result based on the algorithm #2

The system based on the algorithm#2 is tested by the test data and scenarios as same as in the system based on the algorithm#1. An example interpretation of the partial test result for scenario #5 is shown on figure 11 and all the test result is summarized in table 2. For 96 test samples, the system interprets correctly all samples. The algorithm#2 has accurate

interpretation both for condition where the trained and the training object have same and different environmental condition

TABLE II
THE TEST RESULT BASED ON THE ALGORITHM #2

Sc#n DUT	Sc#0	Sc#1	Sc#2	Sc#3	Sc #4	Sc#5	Sc#6	Sc#7
TRI_8	true	true	true	true	true	true	true	true
TRI_9	true	true	true	true	true	true	true	true
TRI_21	true	true	true	true	true	true	true	true
TRI_22	true	true	true	true	true	true	true	true
CIR_8	true	true	true	true	true	true	true	true
CIR_9	true	true	true	true	true	true	true	true
CIR_21	true	true	true	true	true	true	true	true
CIR_22	true	true	true	true	true	true	true	true
REC_8	true	true	true	true	true	true	true	true
REC_9	true	true	true	true	true	true	true	true
REC_21	true	true	true	true	true	true	true	true
REC_22	true	true	true	true	true	true	true	true

B. Visualization of the output result

Generation of the object visual can be done by executed the ResultShower.jar program. The program converts the output decision of C.45 in text form to visual pattern form to show the visual of the tested unknown object. Fig 12 shown an example of the result

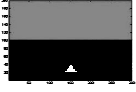
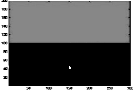
Device Under Test	Results of the interpretation
	D:\ALGORTM#2>T.exe -f training training.ah TRI#0_21_55.tst C4.5 [release 8] decision tree interpreter Mon Mar 16 12:54:50 2009 ----- s: inserting 0.930000 Decision: TRIANGULAR CF = 1.00 [0.88 - 1.00]
	D:\ALGORTM#2>T.exe -f training training.ah CIR#0_8_55.tst C4.5 [release 8] decision tree interpreter Mon Mar 16 12:53:42 2009 ----- s: inserting 0.890000 Decision: CIRCULAR CF = 1.00 [0.88 - 1.00]
	D:\ALGORTM#2>T.exe -f training training.ah REC#0_9_55.tst C4.5 [release 8] decision tree interpreter Mon Mar 16 12:53:05 2009 ----- s: inserting 0.830000 Decision: RECTANGULAR CF = 1.00 [0.88 - 1.00]

Fig.11 An example of the partial test result for scenario #5

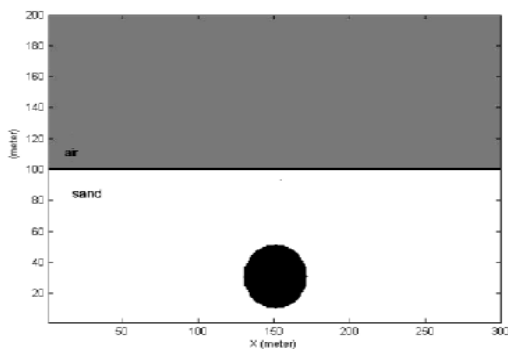


Fig.12 An example of visual output for a circular object

5. Conclusions

In this paper we have proposed a system for identification and interpretation target pattern of buried basic object on surface Ground Penetrating Radar system. Feature parameters of object are extracted by using simple proposed algorithm which based on linear extrapolation. 96 samples of basic object which are laid underground and have both same and different condition with the data training are tested. Results show that all basic objects can be correctly interpreted and the proposed algorithm#2 can improve the performance of system interpretation from 52% to 100%.

References

- [1] Daniels D.J (ed.). "Ground Penetrating Radar" 2nd Edition, *The Institution of Electrical Engineering*, 2004.
- [2] Devaney, A. J., "Geophysical Diffraction Tomography", *IEEE Transactions on Geoscience and Remote Sensing*, Vol. GE-22, NO. 1, pp. 3-13, January 1984.
- [3] Johansson, E.M. and J.E. Mast, "Three-dimensional ground penetrating radar imaging using multi-frequency diffraction tomography", *Advanced Microwave and Millimeter-Wave Detectors, SPIE* Vol. 2275, pp. 196 – 204, July 1994.
- [4] Laksameethanasan.D, "3D Modelling and Imaging based on Transmission Diffraction Tomography and Algebraic Reconstruction Techniques as applied in NDT". *Kassel Univ., Germany*, 2004.
- [5] Aggrawal N. and Karl W.C., "Line Detection in images through Regularized Hough Transform", *IEEE trans. on Image Processing*, vol.15, pp.582-590, 2006.
- [6] Gurbuz A.C., "Feature Detection Algorithms in Computer Images", *Ph.D. Thesis, Georgia Institute of Technology USA*, August 2008.
- [7] Giannopoulos A, "GprMax2D/3D, User's Guide" 2005: <http://www.gprmax.org>.
- [8] Irving J, and Knight R, "Numerical modeling of ground-penetrating radar in 2-D using MATLAB", *Computer & Geosciences, ELSEVIER*, 2005.
- [9] Quinlan, J.R, "C4.5: program for Machine Learning Morgan Kauffman", 1993.
- [10] Irving, J and Knight R, "Numerical simulation of antenna transmission and reception for cross-hole ground-penetrating radar", *Geophysics*, Vol.71, No.2, 2006.
- [11] http://72.14.235.104/search?q=cache:Na5dJVKn0dgJ:cobweb.ecn.purdue.edu/~tmt/ece620/Papers/LaRiviere_TomographyNotes.pdf+tomographic+image+reconstruction&hl=id&ct=clnk&cd=1&gl=id&client=firefox "Tomographic Image Reconstruction".
- [12] Kak.AC and Slaney M, "Principles of Computerized Tomography Imaging", *IEEE Press*, 1987.
- [13] Kunz. K.S and Luebbers. R.J, "The finite difference time domain method for electromagnetic", *CRC Press, London*, 1993.
- [14] Beukelaar.P.et.al, "Locating a buried culvert and the detection of underground cables and pipelines using GPR", *10th European meeting of environmental and engineering geophysics Netherland*, 2004.
- [15] Suksmono A.B., et.al, "A prototype of ultrasound transmission tomography for medical applications", *Image Processing Research Group STEI-ITB*.
- [16] Taflove (ed.), "Advances in computational electrodynamics the finite-difference-time-domain method", *Artech House, London*, 1998.
- [17] Thearling K., "An Introduction to Data Mining" www.thearling.com.
- [18] Xiaoyin, Miller EL, Rappaport C.M., "Statistical method to detect subsurface objects using array ground-penetrating radar data", *IEEE trans on geo-science and remote sensing*, Vol.40, No.2, 2002.
- [19] Youn H.S and Chen CC, "Automatic GPR target detection and clutter reduction using neural network", *Electro-Science Laboratory, USA*.
- [20] Yufryankov B.A. and Linnikov O.N, "Buried cylinders geometric parameters measurement by means of GPR", *Progress in electromagnetic research symposium, USA*, 2006.